Catalysis Science & Technology

Accepted Manuscript

ROYAL SOCIETY OF CHEMISTRY

www.rsc.org/catalysis

Catalysis Science & Technology

ARTICLE

The Enantioselectivity in Asymmetric Ketone Hydrogenation Catalyzed by RuH_2(diphosphine)(diamine) Complexes: Insights From a 3D-QSSR and DFT Study

Received 00th January 20xx,
Accepted 00th January 20xx

DOI: 10.1039/x0xx00000x

www.rsc.org/

Longfei Li[‡ a], Yuhui Pan[‡ a], and Ming Lei[* a]

The three-dimensional quantitative structure-selectivity relationship (3D-QSSR) model was developed to investigate the enantioselectivity of the asymmetric ketone hydrogenation (AKH) catalyzed by RuH_2(diphosphine)(diamine) complexes, through the comparative molecular field analysis (CoMFA). The predicted enantiomeric excess (*ee*) of chiral alcohol products were in good agreement with experimental ones, and the developed model showed good statistics in terms of correlation coefficients (q^2=0.798, r^2=0.996). The predictive power of developed 3D-QSSR model was furtherly proved by test set of 5 ruthenium complexes, with r^2 of 0.974. The contour maps analysis illustrated the sterically and electrostatically favored regions of ruthenium catalysts for improving the enantioselectivity of asymmetric hydrogenation. Under the guidance of the model, we modified the structure of the catalyst RuH_2[(*S*)-tolbinap][(*S*,*S*)-dpen] (**A1**) to the structure RuH_2[(*S*)-tolbinap][(*S*,*S*)-dpen-NH_2] (**C1**) where the aromatic rings of the dpen are substituted with amino groups in the para position. The theoretically predicted catalyst **C1** shows a theoretically calculated increase in ee of AKH by 6.2%. In addition, a computational validation was performed for the catalyst **C1** in the density function theory (DFT), and a larger calculated difference of energy barriers in the hydrogen transfer step accounted for the enhanced enantioselectivity. In conclusion, the 3D-QSSR method could provide a plausible design criterion for the homogeneous transition-metal (TM) catalysts of asymmetric hydrogenation.

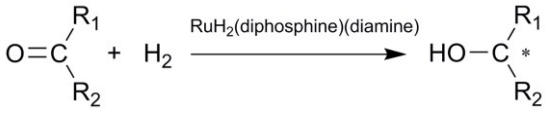

Scheme 1. The asymmetric ketone hydrogenation reaction (AKH) catalyzed by RuH_2(diphosphine)(diamine).

1. Introduction

Since the first successful commercial asymmetric product L-DOPA was synthesized by Monsanto, asymmetric hydrogenation (AH) has been one of the most widely used synthesis methods to produce chiral products.[1] One of the greatest asymmetric products is chiral alcohol, which is exceedingly important building blocks in fine chemistry, pharmacy, agrochemistry, functional materials and so on.[2-6] In the last three decades, the asymmetric ketone hydrogenation (AKH) reactions catalyzed by RuH_2(diphosphine)(diamine) complexes as depicted in Scheme 1 have been reported by experimental and theoretical studies.[6-14] The outer-sphere AKH mechanism through the metal-ligand (M-L) cooperative action is responsible for most of AKH systems.[15-19] The catalytic cycle of AKH could be divided into two steps: (1) the hydrogen transfers to ketone substrates, (2) the catalytic species regeneration via the hydrogenation involving H_2-hydrogenation or transfer hydrogenation.[19-26] Recently, the catalysts based on earth abundant metals like iron and cobalt are paid more and more attention due to the economic and health issues caused by the precious metal catalysts such as ruthenium and rhodium.[4, 27-29] In 2004, Gao *et al*. reported asymmetric transfer hydrogenation catalyzed by the iron complexes with tetradentate P-N-N-P ligands.[30] In 2013, Morris *et al*. developed well-defined iron

[a] *State Key Laboratory of Chemical Resource Engineering, Institute of Materia Medica, College of Science, Beijing University of Chemical Technology, Beijing, 100029, China. Email: leim@mail.buct.edu.cn*
‡ *co-first author*
Electronic Supplementary Information (ESI) available: See DOI: 10.1039/x0xx00000x

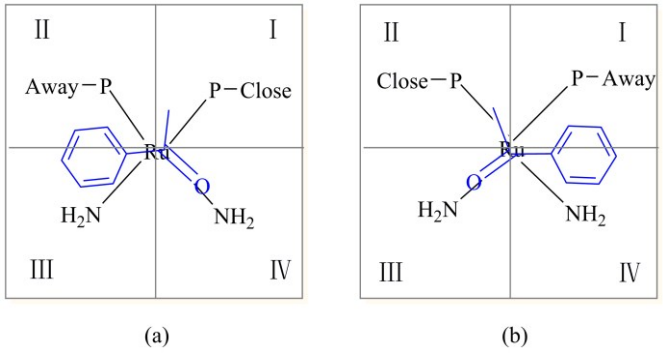

Scheme 2. Four quadrant model in AKHs catalyzed by (a) matched *S*, *SS* or *R*, *RR*-RuH_2(diphosphine)(diamine) and (b) mismatched *S*, *RR* or *R*, *SS*-RuH_2(diphosphine)(diamine) which is used to predict the chirality of the alcohol product.

catalysts for AKH, which could catalyze H_2-hydrogenation or transfer hydrogenation.[31]

Although the mechanisms and origins of enantioselectivity in AKHs catalyzed by Ru catalysts with different structural frameworks were widely studied in detail, the catalyst design is still a challenging work for chemists, which usually need considerable synthetic efforts and empirical science.[32] As we know, the enantioselectivity is dependent on the nature of prochiral ketone substrates, transition-metal center, ligands of catalysts, and the reaction parameters such as pressure, temperature, solvent etc.[33, 34] As for the microenvironment of substituent groups of ketones, aromatic-alkyl ketones have high enantiomeric excess (*ee*) values in AKHs while those of dialkyl ketones have low enantiomeric excess (*ee*) values.[35] The larger alkyl substituent group of aromatic-alkyl ketones lead to the lower enantioselectivity in AKHs catalyzed by BINOL-derived ruthenium complexes.[33] Electron-withdrawing substituents in the para position of the phenyl group of acetophenone result in a low enantioselectivity of AKHs as well.[25] Noyori *et al*. studied the chemoselectivity of olefinic ketones, which arises from the electrophilic and nucleophilic reactivity of the olefinic ketones.[15] The enantioselectivity is dramatically affected by the stereochemical structure of catalyst, and the electronic and steric properties of the diphosphine and diamine ligands play a important role.[1] Such as replacing the chiral dipyridylphosphane ligands (*R*)-P-Phos or (*R*)-Tol-P-Phos with (*R*)-Xyl-P-Phos (Figure 1) is helpful to obtain a higher *ee* value due to the so-called "3,5-dialkyl meta-effect".[36, 37] Besides, ligands' steric effects are clearly reflected in the "V-shape channel" of TolBINAP's Ar_{ax}-P-Ar_{eq} structure in AKHs of aromatic ketones catalyzed by ruthenium complexes. In addition to the diphosphine ligand, the diamine ligand play a critical role as well, such as a replacement of dpen ligand with daipen ligand in RuH_2(diphosphine)(diamine) catalyst could improve the enantioselectivity. Therefore, proper steric and electronic effects between catalyst and substrates could make *R*/*S* reaction pathway more favored than another and contribute the higher enantioselectivity, which is the central issue in AKHs.[38] Some deep mechanistic studies about the enantioselectivity in AKHs have also been reported, and the hydrogen transfer step from catalyst to the ketone substrate was suggested to be the chirality-determining step in the whole catalytic cycle.[5, 16, 20-22, 39-43]

There is an increasing demand to set up a precise model to fully consider the steric and electrostatic effects and achieve the quantitative prediction for the *ee* of AHK catalyzed by transition-metal (TM) complexes with specific structure.[32] The four quadrant theory is largely used in predicting the chirality of produced alcohol since it was raised by Pino and Consiglio. In this method, researchers use a four quadrant model (Scheme 2) to predict the favored chiral alcohol product.[37, 44] However, the four quadrant model is a crude model with considering the steric effects only, that it can just be used for describing the relationship between the catalyst structure and enantioselectivity qualitatively. Catlow *et al*. had made achievement and significance efforts in predicting the enantiomeric excess in AH reactions catalyzed by the Noyori-type catalysts.[45, 46] Given the accuracy of density functional theory (DFT), they performed a mechanistic calculation on the two most favored reaction pathways catalyzed by RuH_2(diphosphine)(diamine) complexes with the diphosphine and diamine ligands bearing different substituents. They found that the difference of the calculated activation energies (ΔE_a) between two most favored (*S*) and (*R*) reaction pathways correlated well with *ee* values, which implies the reliability of this method involving accurate DFT calculations to predict the *ee* of AKHs catalyzed by different catalysts with the same structural framework. In addition, Catlow *et al*. predicted the efficiency of the emerging Fe-based catalysts $Fe^{II}(H)_2$[(*S*)-xylbinap][(*S*,*S*)-dpen] in AKHs compared to the traditional Ru-based catalysts $Ru^{II}(H)_2$[(*S*)-xylbinap][(*S*,*S*)-dpen].[23] However, the expensive and comprehensive analysis using DFT method is not convenient for a large number of catalyst/substrate combinations, although the objects confined to the medium-sized systems more or less routine. Brown and Deeth have proposed a computationally efficient quantum-guided MM method that might be a powerful tool for the catalyst design and refinement.[32] In this context, we supposed the three-dimensional quantitative structure-property relationship (3D-QSPR), a method correlating molecular field descriptors for a set of well-defined chemical compounds with the target property through the statistical analysis of partial least squares (PLS) regression,[47] could offer a precise, rapid and straightforward model for predicting the *ee* in AKHs by the Noyori-type catalysts.

Three-dimensional quantitative structure-activity relationship (3D-QSAR) is widely used for screening new drug candidates, by correlating between biological activities of drugs and molecule structures.[48, 49] Xie's group performed an 3D-QSAR study on a set of arylpyrazole cannabinoid receptor antagonists and designed later-generation analogues of the CB1 and CB2 receptor successfully with the help of the built model.[50] Lei's group investigated a number of small molecules like 2-arylbenzoxazoles (ABZ) analogues proposed as promising therapeutic strategy to treat amyloidosis, and built a 3D-QSAR model that is useful for designing novel TTR amyloidogenesis inhibitors.[51] Xi's group reported a QSAR study of herbicidal sulfonylurea analogues, and defined a general quantumchemical descriptor by characterizing the volume of the electron cloud for specific substituent in the method of density functional theory.[52]

As for the field of catalysis, Cruz's group first applied the 3D-QSAR method to olefin polymerisation catalyzed by ansa-zirconocene and bis(imino)pyridine iron catalysts. The molecular activity and polymer's molecular weights predicted by CoMFA models correlated well with the experimental results, and modifications of the substituents of the aryl rings showed a positive influence as predicted. [47, 53, 54] In Morao's group, the 3D-QSSR method was employed in predicting the *ee* of AKH by three different asymmetric catalysts (L^0-$CuCl_2$, L^{-1}-ZnEt, and L^{-2}-BH) with a good agreement between predictions and experimental data.[55] James *et al*. built a 3D-QSSR model for predicting the *ee* in the β-aminoalkoxide-catalyzed addition-of Et_2Zn to benzaldehyde with a high degree of accuracy.[56] Aguado-Ullate *el al*. investigated the enantioselectivity in the cyclopropanation of styrene catalyzed copper complexes by means of 3D-QSSR, and found the relationship between the enantioselectivity and the steric size of substituents is not strictly linear due to some interplay between substituent effects.[57]

In order to investigate and predict the enantioselectivity in AKHs, we established a 3D-QSSR model for Noyori-type catalysts. 25 RuH_2(diphosphine)(diamine) complexes with exact experimental *ee,*[15] were divided into two subsets as depicted in Table 1. The training set containing 20 catalysts are used for building the model, and the test set containing 5 catalysts for an external validation to confirm the validity of the built model. The provided r^2 represents the prediction ability of the developed model.[55] Based on contour maps generated in CoMFA model, we modified a catalyst and predicted an increase in *ee* for the new catalyst. Considering the reliability of DFT in predicting the enantioselectivity in AKHs,[35, 37, 45, 46] we performed a computational validation for the increase *ee* of AKH by modified catalyst compared with original catalyst using DFT method.

2. Computational Method

2.1 Optimization of molecules

In this paper, we chose 25 ruthenium catalysts (Figure 1) to set up and validate the 3D-QSSR models with the data of these catalysts obtained from literatures.[58-62] All DFT calculations have been carried out in Gaussian 09 program package.[63] In order to guarantee the accuracy, geometry optimizations without any simplification is performed with B3LYP hybrid density functional.[64, 65] The effective core potential of Ru with a double-ζ valence basis set (LANL2DZ) was chosen to describe Ru, and the 6-31G* basis set for other non-metallic atoms (abbreviated in BSI)[66] at the ωB97XD/BSI level.[67] All the transition states (**TS**s) were further confirmed by vibrational analysis and characterized by only one imaginary frequency. All potential energies were corrected for zero-point energy (ZPE) contributions, and Gibbs free energies were calculated at 298.15 K.

2.2 Molecular alignment

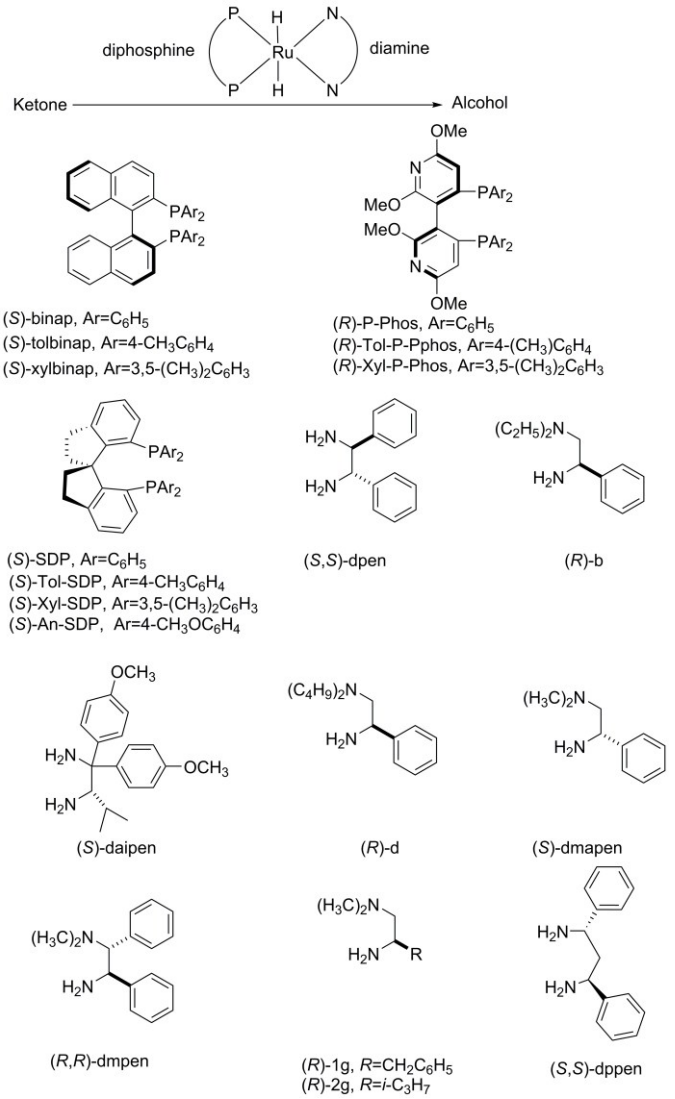

Figure 1. The skeletal structures of catalyst molecules. (The diphosphine and diamine ligands are present in one enantiomer with the other enantiomer omitted.)

All the 3D-QSSR analyses were performed on the CoMFA module implemented in SYBYL-x 1.3 package.[68] The step of molecular alignment is the precondition for the following comparative analysis in 3D-QSSR study, with generating a common structure as the alignment structure.[69, 70] In this step, all of the structures of the ruthenium complexes were oriented as closely as possible with the five atoms (a ruthenium atom, two phosphorus atoms and two nitrogen atoms) chosen to align the structures.

2.3 3D-QSSR approach

The 3D-QSSR method can fully consider the three-dimensional structural information of molecules, based on the analysis of CoMFA. In the CoMFA process, the structures in the common framework are put into a large enough Cartesian lattice with regularly arranged mesh grids, in which critical local differences are identified by sampling field intensities.[71] The sp^3-hybridized carbon atom with a van der Waals radius of 1.52 Å and a charge of +1.0 was selected as probe atom to calculate steric (Lennard-Jones potential) filed energy and electrostatic (Coulombic potential) field with a distance-dependent dielectric.[72-75] For each particular mesh grid, the steric and electrostatic field energy between the probe atom and the catalyst molecule will be calculated and taken as independent variable. The molecular field descriptors was set as Tripos standard, H-bond and Indicator respectively in this study.[48, 74] Tripos standard field is used to describe the steric and electrostatic potentials, and H-bond field is used to describe H-bond potentials in SYBYL-x 1.3 package. Indicator fields replace all lattice energies with magnitudes below a designated threshold with zero values.[75] The partial least squares (PLS), a powerful statistical method, is performed for the combinations of fields and *ee* to establish the 3D-QSSR model.[76, 77] In the process of PLS, the leave-one-out (LOO) cross-validation analysis is firstly carried out with obtaining the cross-validated regression coefficient (q^2) and the optimum number of PLS components. The statistics (q^2) is used for assessing the robustness of the model (q^2= 1-PRESS/$\sum$(Y-Y_{mean})^2, where PRESS = $\sum$(Y-Y_{pred})^2). On this basis, the non-cross-validated conventional analysis is performed to build the final model. The correlation coefficient r^2 and the standard errors of estimate (*SEE*) are obtained consequently, which could assess the predictive ability of the 3D-QSSR model.

3. Results and discussion

3.1 3D-QSSR study on 25 Ru-complexes

This part provides a detailed discussion about the 3D-QSSR study including its establishment, validation, and application to unveil the relationship between structures of ruthenium catalysts and corresponding *ee* of AKHs. The training set comprising 20 ruthenium catalysts were used for building the 3D-QSSR model, and the other 5 species were used for an external validation in order to assess the model's predictive capacity. The diphosphine and diamine ligands involved in this study were listed in Figure 1. The experimental and predicted *ee* of the 25 well-established structures of RuH_2(diphosphine)(diamine) complexes are present in Table 1. The *ee* is positive for the product in *R* conformation, and negative for S conformation. According to the 3D-QSSR model, we introduced amino groups into the phenyl ring of the amine ligand for the catalyst RuH_2[(*S*)-tolbinap][(*S*,*S*)-dpen] (**A1**) and obtained the modified complex RuH_2[(*S*)-tolbinap][(*S*,*S*)-dpen-NH_2] (**C1**) which are shown in Figure 4.

The leave-one-out (LOO) cross-validated PLS analysis was initially carried out. The achieved q^2 is 0.798, and the optimum number of components obtained is 8. Based on this, none-cross-validated PLS analysis was performed to build the final model and the obtained r^2 for the training set is 0.996. The predicted *ee* against experimental

Table 1. The experimental enatioselectivities of catalyst molecules and the predicted values from CoMFA analysis

Catalysts	ee exp.	Config exp.	ee pred.	set
RuH_2[(*R*)-P-Phos][(*R*,*R*)-dpen]	-83	*S*	-77.7	Training
RuH_2[(*R*)-P-Phos][(*S*,*S*)-dppen]	-36	*S*	-33.2	Training
RuH_2[(*R*)-Tol-P-Phos][(*R*,*R*)-dpen]	-82	*S*	-86.6	Training
RuH_2[(*R*)-Xyl-P-Phos][(*S*,*S*)-dppen]	-95	*S*	-102.7	Training
RuH_2[(*S*)-binap][(*S*)-daipen]	87	*R*	87.4	Training
RuH_2[(*S*)-binap][(*S*,*S*)-dpen]	80	*R*	77.7	Training
RuH_2[(*S*)-SDP][(*R*,*R*)-dpen]	-90	*S*	-86.1	Training
RuH_2[(*S*)-tolbinap][(*R*)-1g]	-84	*S*	-81.9	Training
RuH_2[(*S*)-tolbinap][(*R*)-2g]	-82	*S*	-83.5	Training
RuH_2[(*S*)-tolbinap][(*R*)-b]	31	*R*	18.6	Training
RuH_2[(*S*)-tolbinap][(*R*)-d]	26	*R*	34.4	Training
RuH_2[(*S*)-tolbinap][(*R*)-dmapen]	-91	*S*	-86.5	Training
RuH_2[(*S*)-tolbinap][(*R*,*R*)-dmpen]	-79	*S*	-77.0	Training
RuH_2[(*S*)-tolbinap][(*S*)-daipen]	91	*R*	89.1	Training
RuH_2[(*S*)-tolbinap][(*S*,*S*)-dpen]	82	*R*	78.1	Training
RuH_2[(*S*)-tolbinap][(*S*,*S*)-dmpen]	22	*R*	20.0	Training
RuH_2[(*S*)-xylbinap][(*S*)-daipen]	99	*R*	101.1	Training
RuH_2[(*S*)-xylbinap][(*S*,*S*)-dpen]	99	*R*	103.8	Training
RuH_2[(*S*)-Xyl-P-Phos][(*S*,*S*)-dppen]	69	*R*	69.9	Training
RuH_2[(*S*)-Xyl-SDP][(*R*,*R*)-dpen]	-99	*S*	-99.9	Training
RuH_2[(*R*)-Tol-P-Pphos][(*R*,*R*)-dpen]	-85	*S*	-88.9	Test
RuH_2[(*R*)-Xyl-P-Phos][(R,R)-dpen]	-99	*S*	-119.4	Test
RuH_2[(*S*)-tolbinap][(*S*)-dmapen]	-43	*S*	-19.2	Test
RuH_2[(*S*)-Tol-SDP][(*R*,*R*)-dpen]	-92	*S*	-90.1	Test
RuH_2[(*S*)-An-SDP][(*R*,*R*)-dpen]	-89	*S*	-89.8	Test

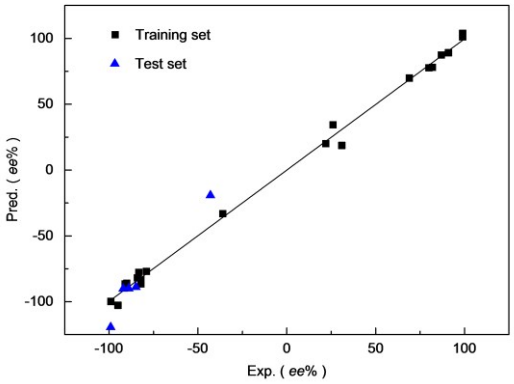

Figure 2. Predicted *ee* by the developed 3D-QSSR model versus experimental *ee* of catalysts. The squares represents the training set data and the triangles represent the test set data.

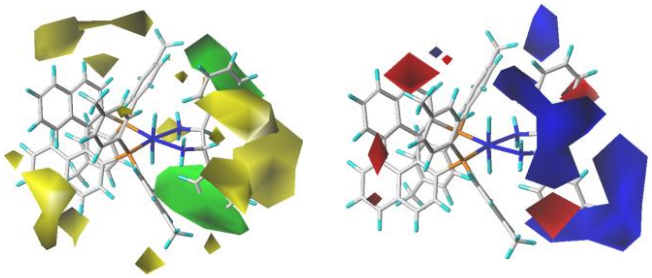

Figure 3. Steric (a) and electrostatic (b) contour maps from CoMFA of catalysts.

ee were plotted in Figure 2, which indicates a good correlation. Besides, a good separation for the *R* products and *S* products is observed, which come together on the upper right hand corner and lower left hand corner respectively. The developed 3D-QSSR model was further tested by 5 complexes in the test set for an external validation, and the predicted *ee* agreed well with experimental *ee*. The obtained r^2 for test set is 0.974, which validates the predictive capacity of the model.

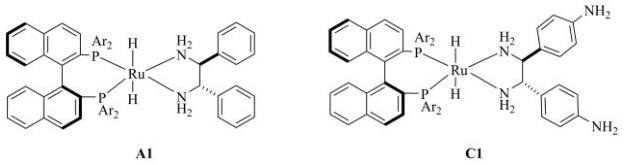

Figure 4. The structures of original catalyst RuH_2[(*S*)-tolbinap][(*S*,*S*)-dpen] (**A1**) (*ee*=78.1%) and modified catalyst RuH_2[(*S*)-tolbinap][(*S*,*S*)-dpen-NH_2] (**C1**) (*ee*=84.3%) (Ar = $CH_3C_6H_4$).

The CoMFA results are graphically described by equipotential surfaces in contour maps. For the sake of clarity, only one catalyst (**A1**) was described in Figure 3. The contributions of steric and electrostatic fields to *ee* are 80.0% and 20.0% respectively. The stdv×coeff field in Figure 3a shows the contribution of steric field in the CoMFA model. The green parts of the equipotential surfaces represent steric favored areas, in which an increase in steric hindrance will be advantageous to get higher *ee* value. On the contrary, the yellow areas represent steric disfavored regions where steric hindrance has a negative impact on the *ee* value of alcohol products. The green contour is mainly concentrated on the amine ligands where an increased steric hindrance is beneficial to produce chiral alcohol with R configuration in ketone hydrogenation. In Figure 3b, the stdev×β shows the contribution of the electrostatic field. If negative charge groups are introduced in the red zone or positive charged groups are introduced in the blue zone, the selectivity of the catalysts will be improved as well. The red zone is mainly concentrated on the phenyl ring of the amine ligand as well.

In short, inspection of the steric and electrostatic fields in the CoMFA model gives instructions to modify the catalysts' structures, and steric favored areas and electrostatically favored areas are mainly in the amine ligand areas. The para C in one of two phenyl groups owns blue contour, suggesting an increase of positive charge of the C will contribute to a higher ee. While the para C in the other phenyl group doesn't own blue contour or red contour, suggesting a charge change of the C will not influence the ee (see the 3D-QSAR videos in SI). Therefore, we introduced amino groups in both *para* positions of phenyl moiety of amine ligands of **A1** to get **C1** catalyst (Figure 4), which lead to an increased *ee* of 84.3% in AKH using the

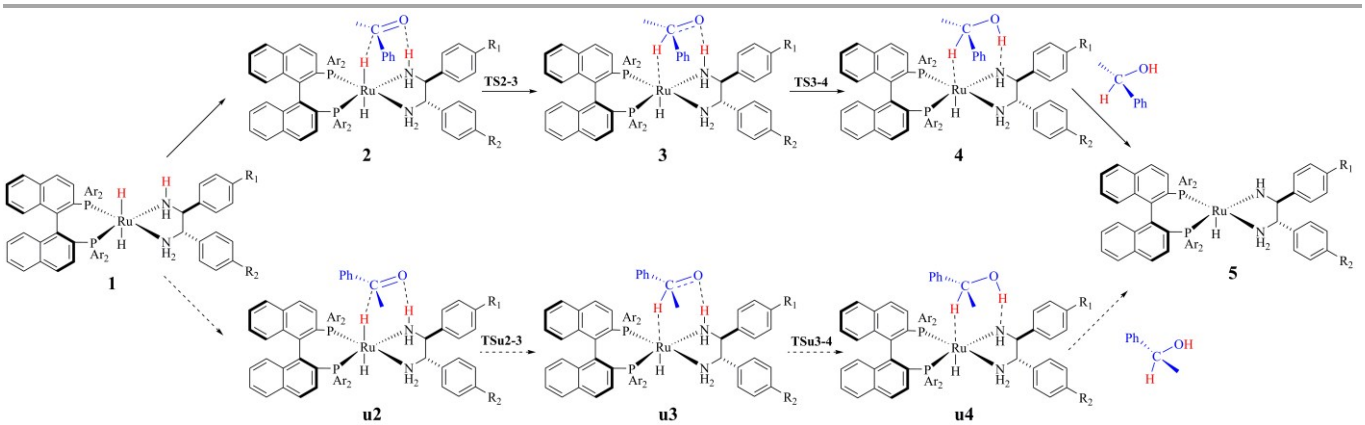

Figure 5. The hydrogen transfer step catalyzed by RuH_2(*S*-tolbinap)(*S*,*S*-dpen) catalysts with different 1,2-diaryldiamine ligands substituted in the para position with groups R1 and R2 (A: R_1 = H, R_2 = H; C: R_1 = NH_2, R_2 = NH_2). The $CH_3C_6H_4$ was simplified as Ar. The lower energy route for producing R configuration alcohol was shown in solid arrows. The higher energy route for creating S configuration alcohols was shown in dotted arrows.

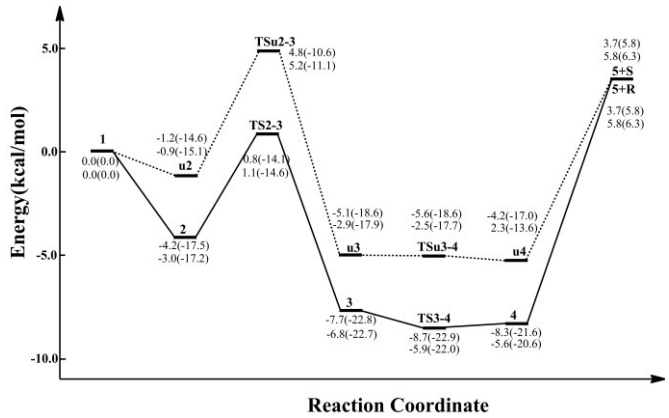

Figure 6. Energy profiles of acetophenone catalyzed by **A1** and **C1** at the ωB97X-D/BSI level. (The solid lines denotes the favourable pathway for producing *R* configuration phenethyl alcohol, and the dotted lines describes the disadvantage route for *S* configuration product. The energy out of the parentheses is free energy and the potential energy is in the parentheses. The energy data from top to bottom correspond to catalysts **A** and **C**. unit: kcal/mol)

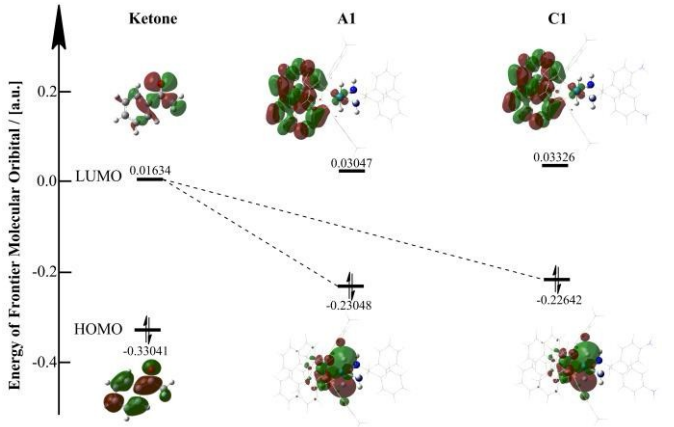

Figure 7. Interaction in frontier molecular orbitals (FMOs) of acetophenone and complexes **A1** and **C1**.

3D-QSSR study above. The APT charges of para C in the two phenyl groups of the starting catalyst **A1** are -0.033 and -0.033, respectively. And those of the modified catalyst **C1** change to 0.608 and 0.612, respectively.

3.2 The analysis of the new modified catalyst.

The mechanism of ketone hydrogenation catalyzed by RuH_2(diphosphine)(diamine) was proposed by Noyori and co-workers. Tommaso's group found that there were two most likely coordination modes for pseudo reaction coordinate Ru-H···C=O of trans-RuH_2(*S*,*S*-dpen)(*S*-tolbinap) which are depicted in **SI**.[37] As shown in Figure 5, the AKH catalyzed by the 18-electron dihydride complex **1** provides favored (*R*)-phenethyl alcohol and disfavored (*S*)-phenethyl alcohol through two different pathways. The substrate acetophenone to the outer coordination sphere of the dihydride complex **1** with generating the intermediates **2** and **u2**, leading to the mentioned two different chiral products. Taking the favored intermediates **2** for granted, the hydride transfers from the Ru to carbon via the transition state **TS2-3** generating the intermediates **3**. Then, the proton transfers from nitrogen to the oxygen via **TS3-4** providing the intermediate **4**. Subsequently, the favored (*R*)-phenethyl alcohol is released, with forming the 16-electron Ru-amido metal species **5**. The active species **1** is regenerated through a heterolytic splitting of dihydrogen under the species **5**. Hydride transfer step from the Ru complex to the ketone substrate is the chirality-determining step.[78] As for the modified catalyst (**C1**) and original one (**A1**), we performed a DFT calculation and correlated the energy barrier difference of HT steps in reaction pathways to *S/R* alcohols and the *ee* values, which could further investigate the nature of *ee* increase by means of the modification of catalyst **A1**.

Figure 6 displays the free energy profiles for the original catalyst **A1** and new modified catalyst **C1**. In the chirality-determining step of hydrogen transfer step, the energy barriers of **A1** is 5.0 (3.4) kcal/mol in (*R*) reaction pathway, and 6.0 (4.0) kcal/mol in (*S*) reaction pathway, with a free energy difference (Δ*ΔG*) of 1.0 (0.6) kcal/mol. The corresponding energy barriers in AKH by catalyst **C1** are 4.1 (2.6) kcal/mol in (*R*) reaction pathway and 6.1 (4.0) kcal/mol in (*S*) reaction pathway respectively, with a *ΔΔG* of 2.0 (1.4) kcal/mol which is larger than that in AKH using **A1**. In AKH of acetophenone catalyzed by complex **A1** or **C1**, (*R*)-phenethyl alcohol is the main product. And the modified catalyst, the complex **C1**, is the better catalyst in enantioselectivity according to the analysis of the free energy and potential energy differences, which are in consist with the 3D-QSSR results.

The interaction of frontier molecular orbitals (FMOs) between acetophenone and dihydride complexes is shown in Figure 7. It is known that hydride transfers from dihydride complexes **A1** and **C1** to acetophenone. The gaps between LUMO of acetophenone and HOMO of catalyst **C1** is smaller in contrast to the catalyst **A1**. This also indicates that it's easier for hydride to transfer from complex **C1** to acetophone. Previous studies pointed out that the steric effects between the two substituent groups of the ketone and achiral ligands of catalysts play an important role in the enantioselectivity of AKHs.[35, 41, 79] This DFT study demonstrates the important role of electrostatic effect. The APT charges of $H^{\delta-}$ in $H^{\delta+}$–$N^{\delta-}$---$Ru^{\delta+}$–$H^{\delta-}$ moiety of the 18e dihydride species **2** and **u2** are -0.227 and -0.230 for **A1** system, while -0.229 and -0.228 for **C1** system. Those of Ru in H–N---Ru–H moiety of **2** and **u2** are -0.981 and -0.972 for **A1** system, while -0.993 and -0.976 for **C1** system. The differences in charge (CDs) between Ru center and $H^{\delta-}$ are 0.754 and 0.741 for **2** and **u2** in **A1** system respectively (CD= charge of $H^{\delta-}$ minus charge of Ru). And those are 0.764 and 0.748 in **C1** system, respectively. The CDs agree well with DFT calculation, which implies the important role of hydride transfer step in the entioselectivity of AKHs, and a larger CD will lead to a lower energy barrier of hydride transfer. The change of CD for **C1** system is due to the inductive electron-donating effect of NH_2 introduction in *para*-position of phenyl ring of amine ligand.

4. Conclusions

3D-QSSR, as a fast and low-cost method was used to predict the *ee* of the RuH_2(diphosphine)(diamine) catalysts in this paper, which provided a detail insight into the structure-enantioselectivity

relationship. The statistical model was derived with the CoMFA method, based on structurally diverse catalysts in the training set including bifunctional and spiro catalysts. The generated model showed good statistical correlation in terms of q^2=0.798, r^2=0.996, and the predicted *ee* values in AKHs were in excellent agreement with experimental results. The statistical significance and robustness of established model were judged by the test set. The spatial effect of the steric and electrostatic fields were visually given by the contour map, which indicates how the structures influence the enantioselectivity of AKHs by RuH_2(diphosphine)(diamine) complexes. In addition, we introduced amino group (-NH_2) into each phenyl ring of the amine ligand, and the modified AKH catalyst **C1** was found to produce 1-phenylethanol with an improved *ee* value compared with that of the original catalyst **A1**. Then, this modification was verified by the DFT study and was accounted for an enhanced difference of energy barriers of the HT steps in (*S*) and (*R*) reaction pathways. These results indicate the method of 3D-QSSR is an accurate and straightforward alignment-independent approach for the prediction of the *ee* in AKHs, and give guidelines for modifying the Ru catalysts in this study. What is more, the method could potentially assist the design of other homogeneous transition-metal catalysts in an efficient, money-saving way.

Acknowledgements

This work was in part supported by the National Natural Science Foundation of China (Grant No. 21373023), BUCT Fund for Disciplines Construction and Development (Project No. XK1527). We also thank National Supercomputing Center in Shenzhen (NSCCSZ) for providing a part of the computational resources.

Notes and references

1. W. S. Knowles and R. Noyori, *Acc. Chem. Res.*, 2007, **40**, 1238-1239.
2. H. Blaser, F. Spindler and M. Studer, *Appl. Catal. A. Gen.*, 2001, **221**, 119-143.
3. N. B. Johnson, I. C. Lennon, P. H. Moran and J. A. Ramsden, *Acc. Chem. Res.*, 2007, **40**, 1291-1299.
4. R. H. Morris, *Acc. Chem. Res.*, 2015, **48**, 1494-1502.
5. R. Noyori and H. Takaya, *Acc. Chem. Res.*, 1990, **23**, 345-350.
6. S. E. Clapham, A. Hadzovic and R. H. Morris, *Coord. Chem. Rev.*, 2004, **248**, 2201-2237.
7. Q. Zhu, D. Shi, C. Xia and H. Huang, *Chem. Eur. J.*, 2011, **17**, 7760-7763.
8. M. Akashi, N. Arai, T. Inoue and T. Ohkuma, *Adv. Synth. Catal.*, 2011, **353**, 1955-1960.
9. O. N. Faza, I. Fernández and C. S. López, *Chem. Commun.*, 2013, **49**, 4277-4279.
10. P. A. Dub, N. J. Henson, R. L. Martin and J. C. Gordon, *J. Am. Chem. Soc.*, 2014, **136**, 3505-3521.
11. S. Rodriguez, B. Qu, K. R. Fandrick, F. Buono, N. Haddad, Y. Xu, M. A. Herbage, X. Zeng, S. Ma and N. Grinberg, *Adv. Synth. Catal.*, 2014, **356**, 301-307.
12. E. Limé, M. D. Lundholm, A. Forbes, O. Wiest, P. Helquist and P.-O. Norrby, *J. Chem. Theory Comput.*, 2014, **10**, 2427-2435.
13. M. Yoshimura, S. Tanaka and M. Kitamura, *Tetrahedron. Lett.*, 2014, **55**, 3635-3640.
14. J.-H. Xie, D.-H. Bao and Q.-L. Zhou, *Synthesis*, 2015, **47**, 460-471.
15. R. Noyori and T. Ohkuma, *Angew. Chem., Int. Ed.*, 2001, **40**, 40-73.
16. R. Noyori, *Angew. Chem., Int. Ed.*, 2002, **41**, 2008-2022.
17. T. Ohkuma, C. A. Sandoval, R. Srinivasan, Q. Lin, Y. Wei, K. Muniz and R. Noyori, *J. Am. Chem. Soc.*, 2005, **127**, 8288-8289.
18. C. Wang, X. Wu and J. Xiao, *Chem. Asian. J.*, 2008, **3**, 1750-1770.
19. R. Abbel, K. Abdur-Rashid, M. Faatz, A. Hadzovic, A. J. Lough and R. H. Morris, *J. Am. Chem. Soc.*, 2005, **127**, 1870-1882.
20. R. Guo, A. J. Lough, R. H. Morris and D. Song, *Organometallics*, 2004, **23**, 5524-5529.
21. Y. Chen, S. Liu and M. Lei, *J. Phys. Chem. C*, 2008, **112**, 13524-13527.
22. Y. Chen, Y. Tang and M. Lei, *Dalton. Trans.*, 2009, 2359-2364.
23. H.-Y. T. Chen, D. Di Tommaso, G. Hogarth and C. R. A. Catlow, *Dalton. Trans.*, 2011, **40**, 402-412.
24. C. Hedberg, K. Källström, P. I. Arvidsson, P. Brandt and P. G. Andersson, *J. Am. Chem. Soc.*, 2005, **127**, 15083-15090.
25. C. A. Sandoval, T. Ohkuma, K. Muñiz and R. Noyori, *J. Am. Chem. Soc.*, 2003, **125**, 13490-13503.
26. R. Noyori, M. Kitamura and T. Ohkuma, *Proc. Natl. Acad. Sci. U.S.A.*, 2004, **101**, 5356-5362.
27. M. R. Friedfeld, M. Shevlin, J. M. Hoyt, S. W. Krska, M. T. Tudge and P. J. Chirik, *Science*, 2013, **342**, 1076-1080.
28. J. S. Anderson, J. Rittle and J. C. Peters, *Nature*, 2013, **501**, 84-+.
29. T.-P. Lin and J. C. Peters, *J. Am. Chem. Soc.*, 2013, **135**, 15310-15313.
30. J. Chen, L. Chen, Y. Xin, G. Chen, W. Shen, Z. Dong, Y. Li and J. Gao, *Acta Chim. Sinica*, 2004, **62**, 1745-1750.
31. W. Zuo, A. J. Lough, Y. F. Li and R. H. Morris, *Science*, 2013, **342**, 1080-1083.
32. J. M. Brown and R. J. Deeth, *Angew. Chem. Int. Edit.*, 2009, **48**, 4476-4479.
33. Y. Xu, G. C. Clarkson, G. Docherty, C. L. North, G. Woodward and M. Wills, *J. Org. Chem.*, 2005, **70**, 8079-8087.
34. S. Subongkoj, S. Lange, W. Chen and J. Xiao, *J. Mol. Catal. A: Chem.*, 2003, **196**, 125-129.
35. R. Feng, A. Xiao, X. Zhang, Y. Tang and M. Lei, *Dalton. Trans.*, 2013, **42**, 2130-2145.
36. J. Wu, J. X. Ji, R. Guo, C. H. Yeung and A. S. Chan, *Chem. Eur. J.*, 2003, **9**, 2963-2968.
37. D. Di Tommaso, S. A. French, A. Zanotti-Gerosa, F. Hancock, E. J. Palin and C. R. A. Catlow, *Inorg. Chem.*, 2008, **47**, 2674-2687.
38. H. Ooka, N. Arai, K. Azuma, N. Kurono and T. Ohkuma, *J. Org. Chem.*, 2008, **73**, 9084-9093.
39. R. Noyori, T. Ohkuma, M. Kitamura, H. Takaya, N. Sayo, H. Kumobayashi and S. Akutagawa, *J. Am. Chem. Soc.*, 1987, **109**, 5856-5858.
40. Y. Chen, Y. Tang, S. Liu, M. Lei and W. Fang, *Organometallics*, 2009, **28**, 2078-2084.
41. Z. Chen, Y. Chen, Y. Tang and M. Lei, *Dalton. Trans.*, 2010, **39**, 2036-2043.

42. X. Guo, Y. Tang, X. Zhang and M. Lei, *J. Phys. Chem. A*, 2011, **115**, 12321-12330.
43. X. Zhang, X. Guo, Y. Chen, Y. Tang, M. Lei and W. Fang, *Phys. Chem. Chem. Phys.*, 2012, **14**, 6003-6012.
44. T. Leyssens, D. Peeters and J. N. Harvey, *Organometallics*, 2008, **27**, 1514-1523.
45. H.-Y. T. Chen, D. Di Tommaso, G. Hogarth and C. R. A. Catlow, *Catal. lett.*, 2011, **141**, 1761-1766.
46. H.-Y. T. Chen, D. Di Tommaso, G. Hogarth and C. R. A. Catlow, *Dalton. Trans.*, 2012, **41**, 1867-1877.
47. V. L. Cruz, S. Martinez, J. Ramos and J. Martinez-Salazar, *Organometallics*, 2014, **33**, 2944-2959.
48. J. Verma, V. M. Khedkar and E. C. Coutinho, *Current Topics in Medicinal Chemistry*, 2010, **10**, 95-115.
49. H. Kubinyi and P. v. R. Schleyer, *Vol. 1John Wiley & Sons Ltd*, 1998, 448-460.
50. J.-Z. Chen, X.-W. Han, Q. Liu, A. Makriyannis, J. Wang and X.-Q. Xie, *J. Med. Chem.*, 2006, **49**, 625-636.
51. L. Zhao, L. Zhang and M. Lei, *Sci. China. Chem.*, 2013, **56**, 1550-1563.
52. Z. Xi, Z. Yu, C. Niu, S. Ban and G. Yang, *J. Comput. Chem.*, 2006, **27**, 1571-1576.
53. V. Cruz, J. Ramos, A. Munoz-Escalona, P. Lafuente, B. Pena and J. Martinez-Salazar, *Polymer*, 2004, **45**, 2061-2072.
54. V. Cruz, J. Martinez, J. Martinez-Salazar, J. Ramos, M. Reyes, A. Toro-Labbe and S. Gutierrez-Oliva, *Polymer*, 2007, **48**, 7672-7678.
55. S. Sciabola, A. Alex, P. D. Higginson, J. C. Mitchell, M. J. Snowden and I. Morao, *J. Org. Chem.*, 2005, **70**, 9025-9027.
56. J. C. Ianni, V. Annamalai, P.-W. Phuan, M. Panda and M. C. Kozlowski, *Angew. Chem.*, 2006, **118**, 5628-5631.
57. S. Aguado‐Ullate, M. Urbano‐Cuadrado, I. Villalba, E. Pires, J. I. García, C. Bo and J. J. Carbó, *Chem. Eur. J.*, 2012, **18**, 14026-14036.
58. J.-H. Xie and Q.-L. Zhou, *Acc. Chem. Res.*, 2008, **41**, 581-593.
59. J. Wu, H. Chen, W. Kwok, R. Guo, Z. Zhou, C. Yeung and A. S. Chan, *J. Org. Chem.*, 2002, **67**, 7908-7910.
60. T. Ohkuma, *Proc. Jpn. Acad. Ser B., Phys. Biol. Sci.*, 2010, **86**, 202.
61. G. A. Grasa, A. Zanotti-Gerosa and W. P. Hems, *Organometallic*, 2006, **691**, 2332-2334.
62. T. Ohkuma, M. Koizumi, K. Muñiz, G. Hilt, C. Kabuto and R. Noyori, *J. Am. Chem. Soc.*, 2002, **124**, 6508-6509.
63. Frisch, M. J.; et al. Gaussian 09, Revision B.01; Gaussian, Inc.:Wallingford, CT, 2010.
64. C. Lee, W. Yang and R. G. Parr, *Phys. Rev. B.*, 1988, **37**, 785-789.
65. A. D. Becke, *J. Chem. Phys.*, 1993, **98**, 5648-5652.
66. P. J. Hay and W. R. Wadt, *J. Chem. Phys.*, 1985, **82**, 299-310.
67. J.-D. Chai and M. Head-Gordon, *PCCP*, 2008, **10**, 6615-6620.
68. M. St. Louis, *SYBYL-X 1.3, Molecular Modeling Software, Tripos Associates,*, 2011.
69. C. Hansch, P. P. Maloney, T. Fujita and R. M. Muir, 1962.
70. C. Martin, K. Kim, C. Lin and M. Charton, *Adv. Quant. Struct.-Prop. Relat.*, 1996.
71. V. L. Cruz, J. Ramos, S. Martinez, A. Muñoz-Escalona and J. Martinez-Salazar, *Organometallics*, 2005, **24**, 5095-5102.
72. G. E. Kellogg, S. F. Semus and D. J. Abraham, *Journal of computer-aided molecular design*, 1991, **5**, 545-552.
73. P. Lu, X. Wei and R. Zhang, *European Journal of Medicinal Chemistry*, 2010, **45**, 3413-3419.
74. J. Sun, S. Cai, N. Yan and H. Mei, *European Journal of Medicinal Chemistry*, 2010, **45**, 1008-1014.
75. T. Liljefors, *Perspectives in drug discovery and design*, 1998, **9**, 3-17.
76. S. Wold, A. Ruhe, H. Wold and I. Dunn, WJ, *SIAM J. Sci. Comput.*, 1984, **5**, 735-743.
77. F. Pelascini, F. Peruch, P. J. Lutz, M. Wesolek and J. Kress, *Eur. Polym. J.*, 2005, **41**, 1288-1295.
78. J. L. Gázquez, A. Vela and M. Galván, in *Electronegativity*, Springer, 1987, pp. 79-97.
79. K. Mikami, T. Korenaga, T. Ohkuma and R. Noyori, *Angew. Chem. Int. Edit.*, 2000, **39**, 3707-3710.

The Enantioselectivity in Asymmetric Ketone Hydrogenation Catalyzed by RuH_2(diphosphine)(diamine) Complexes: Insights From a 3D-QSSR and DFT Study

Longfei Li[‡ a], Yuhui Pan[‡ a], and Ming Lei[* a]

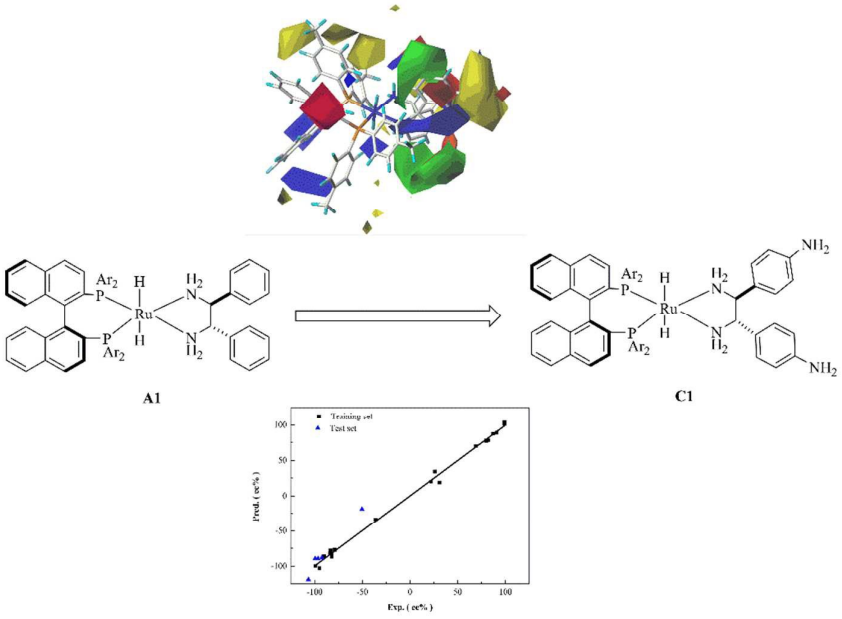

The three-dimensional quantitative structure-selectivity relationship (3D-QSSR) model was developed to investigate the enantioselectivity of the asymmetric ketone hydrogenation (AKH) catalyzed by RuH_2(diphosphine)(diamine) complexes, through the comparative molecular field analysis (CoMFA). The predicted enantiomeric excess (*ee*) of chiral alcohol products were in good agreement with experimental ones, and the developed model showed good statistics in terms of correlation coefficients (q^2=0.798, r^2=0.996). The predictive power of developed 3D-QSSR model was furtherly proved by test set of 5 ruthenium complexes, with r^2 of 0.974. The contour maps analysis illustrated the sterically and electrostatically favored regions of ruthenium catalysts for improving the enantioselectivity of asymmetric hydrogenation. Under the guidance of the model, we modified the structure of the catalyst RuH_2[(*S*)-tolbinap][(*S*,*S*)-dpen] (**A1**) to the structure RuH_2[(*S*)-tolbinap][(*S*,*S*)-dpen-NH_2] (**C1**) where the aromatic rings of the dpen are substituted with amino groups in the para position. The theoretically predicted catalyst **C1** shows a theoretically calculated increase in ee of AKH by 6.2%. In addition, a computational validation was performed for the catalyst **C1** in the density function theory (DFT), and a larger calculated difference of energy barriers in the hydrogen transfer step accounted for the enhanced enantioselectivity. In conclusion, the 3D-QSSR method could provide a plausible design criterion for the homogeneous transition-metal (TM) catalysts of asymmetric hydrogenation.